Control Strategies for Three Phase PWM Rectifier using Space Vector Modulation: Part-II

Jagan Mohana Rao Malla

3. Voltage Oriented Control of PWM Rectifier

3.1 Introduction

The Voltage Oriented Control (*VOC*) for line side PWM rectifier is based on coordinate transformation between stationary α-β and synchronous rotating *d-q* reference system. This strategy guarantees fast transient response and high static performance via an internal current control loops. Consequently, the final configuration and performance of system largely depends on the quality of applied current control strategy .The easiest solution is hysteresis current control that provides a fast dynamic response, good accuracy, no *DC* offset and high robustness. However the major problem of hysteresis control is that its average switching frequency varies with the load current, which makes the switching pattern uneven and random, thus, resulting in additional stress on switching devices and difficulties of LC input filter design. Among regulators the widely used scheme for high performance current control is the *d-q* synchronous controller, where the currents being regulated are *a DC* quantity which eliminates steady state error.

3.2 Voltage Oriented Control (VOC)

The conventional control system uses closed-loop current control in rotating reference frame, the Voltage Oriented Control (*VOC*) scheme is shown in Fig.3.1.

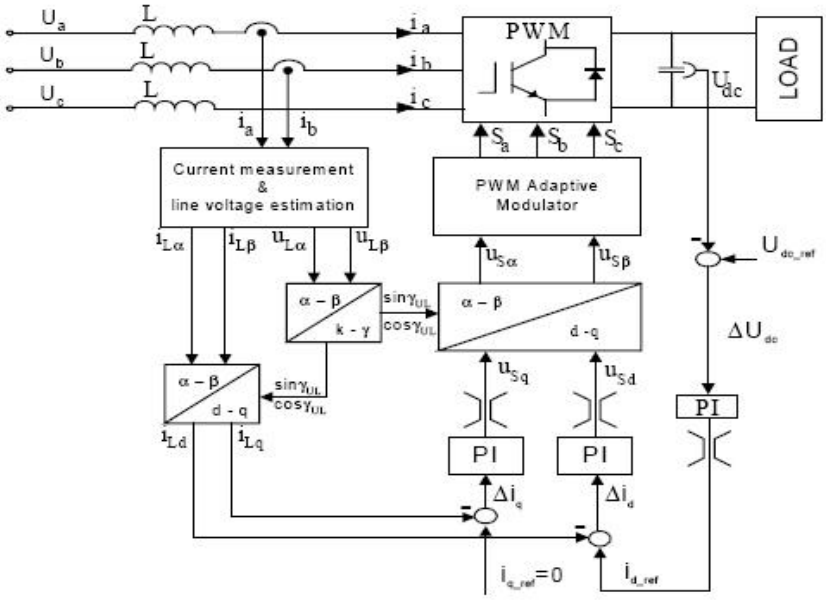

Fig. 3.1 Block scheme of AC voltage sensorless VOC

A characteristic feature for this current controller is processing of signals in two coordinate systems. The first is stationary α-β and the second is synchronously rotating *d-q* coordinate system. Three phase measured values are converted to equivalent two phase system α-β and then are transformed to rotating coordinate system in a block α-β/*d-q*:

$$\begin{bmatrix} kd \\ kq \end{bmatrix} = \begin{bmatrix} \cos\gamma UL & \sin\gamma UL \\ -\sin\gamma UL & \cos\gamma UL \end{bmatrix} \begin{bmatrix} k\alpha \\ k\beta \end{bmatrix} \quad (3.1a)$$

This type of transformation, the control values are DC signals. An inverse transformation *d-q*/α-β is achieved on the output of control system and it gives a result the rectifier reference signals in stationary coordinate:

$$\begin{bmatrix} k\alpha \\ k\beta \end{bmatrix} = \begin{bmatrix} \cos\gamma UL & -\sin\gamma UL \\ \sin\gamma UL & \cos\gamma UL \end{bmatrix} \begin{bmatrix} kd \\ kq \end{bmatrix} \quad (3.1b)$$

For both coordinate transformation the angle of the voltage vector γUL is defined as:

$$\sin\gamma_{UL} = \frac{u_{L\beta}}{\sqrt{u_{L\alpha}^2 + u_{L\beta}^2}} \quad (3.2a)$$

$$\cos\gamma_{UL} = \frac{u_{L\alpha}}{\sqrt{u_{L\alpha}^2 + u_{L\beta}^2}} \quad (3.2b)$$

In voltage oriented *d-q* coordinates, the AC line current vector *iL* is split into two rectangular components *Il = [iLd, iLq]* (Fig. 3.2). The component *iLq* determinates reactive power, whereas *iLd* decides about active power flow. Thus the reactive and the active power can be controlled independently. The *UPF* condition is met when the line current vector, *iL*, is aligned with the line voltage

vector, *uL*. By placing the d-axis of the rotating coordinates on the line voltage vector a simplified dynamic model can be obtained.

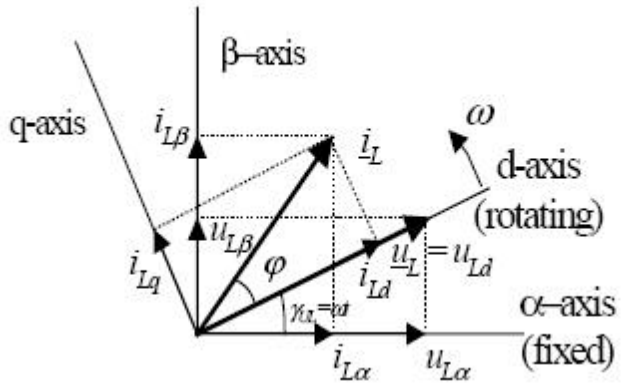

Fig. 3.2: Vector diagram of VOC. Coordinate transformation of line current, line voltage and rectifier input voltage from stationary α−β coordinates to rotating *d-q* coordinates.

The voltage equation in the d-q synchronous reference frame is as follows:

$$u_{Ld} = Ri_{Ld} + L\frac{di_{Ld}}{dt} - \omega Li_{Lq} + u_{Sd} \quad (3.3)$$

$$u_{Lq} = Ri_{Lq} + L\frac{di_{Lq}}{dt} - \omega Li_{Ld} + u_{Sq} \quad (3.4)$$

Regarding to Fig. 3.1, the *q*-axis current is set to zero in all condition for unity power factor control while the reference current *iLd* is set by the DC-link voltage controller and controls the active power flow between the supply and the DC-link. For $R \approx 0$ equations (3.3), (3.4) can be reduced to:

$$u_{Ld} = L\frac{di_{Ld}}{dt} - \omega Li_{Lq} + u_{Sd} \quad (3.5)$$

$$0 = L\frac{di_{Lq}}{dt} - \omega Li_{Ld} + u_{Sq} \quad (3.6)$$

Assuming that the q-axis current is well regulated to zero, the following equations hold true

$$u_{Ld} = L\frac{di_{Ld}}{dt} + u_{Sd} \quad (3.7)$$

$$0 = L\frac{di_{Lq}}{dt} + u_{Sq} \quad (3.8)$$

As current controller, the PI-type can be used. However, the *PI* current controller has no satisfactory tracing performance, especially, for the coupled system described by Eqs. (3.5), (3.6). Therefore for high performance application with accuracy current tracking at dynamic state the decoupled controller diagram for the PWM rectifier should be applied what is shown in Fig. 3.3.

$$u_{Sd} = \omega Li_{Lq} + u_{Sd} + \Delta u_d \quad (3.9)$$

$$0 = -\omega Li_{Ld} + \Delta u_q \quad (3.10)$$

where Δ is the output signals of the current controllers

$$\Delta u_d = k_p (i^*_d - i_d) + k_i \int (i^*_d - i_d)\, dt \quad (3.11)$$

$$\Delta u_q = k_p (i^*_q - i_q) + k_i \int (i^*_q - i_q)\, dt \quad (3.12)$$

The output signals from PI controllers after *dq/αβ* transformation (Eq. (3.1b)) are used for switching signals generation by a Space Vector Modulator.

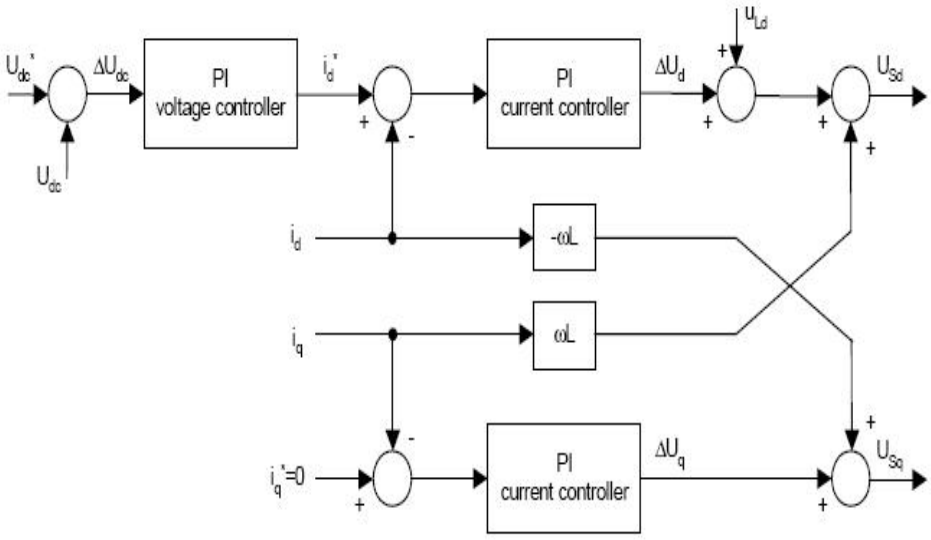

Fig. 3.3 Decoupled current control of PWM rectifier

3.2.1 Line voltage Estimator

An important requirement for a voltage estimator is to estimate the voltage correct also under unbalanced conditions and pre-existing harmonic voltage distortion. Not only the fundamental component should be estimated correct, but also the harmonic components and the voltage unbalance. It gives a higher total power factor. It is possible to calculate the voltage across the inductance by the current differentiating. The line voltage can then be estimated by adding reference of the rectifier input voltage to the

calculated voltage drop across the inductor. However, this approach has the disadvantage that the current is differentiated and noise in the current signal is gained through the differentiation. To prevent this voltage estimator based on the power estimator can be applied. In this current is sampled and the power is estimated several times in every switching state. In conventional space vector modulation (SVM) for three-phase voltage source converters, the *AC* currents are sampled during the zero-vector states because no switching noise is present and a filter in the current feedback for the current control loops can be avoided. Using equation (3.13) and (3.14) the estimated active and reactive power in this special case (zero states) can be expressed as:

$$p = L\left(\frac{di_a}{dt} i_a + \frac{di_b}{dt} i_b + \frac{di_c}{dt} i_c\right) \quad (3.13)$$

$$q = 3L \frac{1}{\sqrt{3}} \left(\frac{di_a}{dt} i_c - \frac{di_c}{dt} i_a\right) \quad (3.14)$$

It should be noted that in this special case it is only possible to estimate the reactive power in the inductor. Since powers are DC-values it is possible to prevent the noise of the differentiated current by use of a simple (digital) low pass filter. This ensures a robust and noise insensitive performance of the voltage estimator. Based on instantaneous power theory, the estimated voltage across the inductance is:

$$\begin{bmatrix} uL\alpha \\ uL\beta \end{bmatrix} = \frac{1}{i_{L\alpha}^2 + i_{L\beta}^2} \begin{bmatrix} iL\alpha - iL\beta \\ iL\beta iL\alpha \end{bmatrix} \begin{bmatrix} p \\ q \end{bmatrix} \quad (3.15)$$

where:

*uIα, uI*β are the estimated values of the three-phase voltages across the inductance *L*, in the fixed α-β coordinates. The estimated line voltage *uL(est)* can now be found by adding the voltage reference of the PWM rectifier to the estimated inductor voltage

$$u_{L(est)} = u_S + u_I \quad (3.16)$$

3.3 Pulse Width Modulation (PWM)

Applications and power converter topologies are still expanding with improvements in semiconductor technology, which offer higher voltage and current rating as well as better switching characteristics. On the other hand, the main advantages of modern power electronic converters such as: high efficiency, low weight and small dimensions, fast operation and high power densities are being achieved through the use of the so called *switch mode operation*, in which power semiconductor devices are controlled in *ON/OFF* fashion. This leads to different types of Pulse Width Modulation (*PWM*), which is basic energy processing technique applied in power converter systems. In modern converters, *PWM* is high-speed process ranging-depending on a rated power from a few kHz (motor control) up to several MHz (resonant converters for power supply). Therefore, an on-line optimization procedure is hard to be implemented especially, for three or multi-phase converters. Fig.3.4. presents three-phase voltage source PWM converter, which is the most popular power conversion circuit used in industry. This topology can work in two modes:

- **Inverter** - when energy, of adjusted amplitude and frequency, is converted from *DC* side to *AC* side. This mode is used in variable speed drives and *AC* power supply including uninterruptible power supply (*UPS*),
- **Rectifier** - when energy of mains (50 Hz or 60Hz) is converted from *AC* side to *DC* side. This mode has application in power supply with Unity Power Factor (*UPF*).

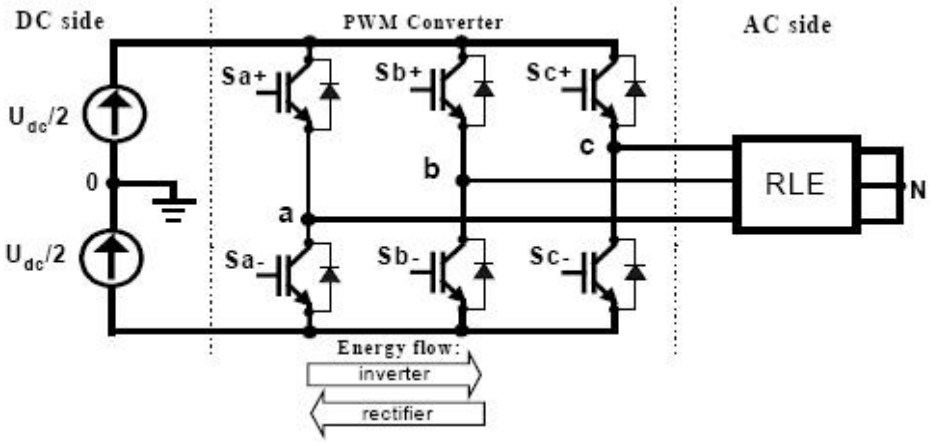

Fig. 3.4. Three-phase voltage source PWM converter

Performance of PWM rectifiers significantly depends on control methods and type of modulation. Therefore the PWM converter should satisfy the following requirements.

- wide range of linear operation,
- Minimal number of (frequency) switching to keep low switching losses in power components
- Low content of higher harmonics in voltage and current, because they produce additional losses and noise in load,
- Elimination of low frequency harmonics (in case of motors it generates torque pulsation)
- Operation in over modulation region including square wave.

Additionally, investigations are lead with the purpose of:

- Simplification because modulator is one of the most time-consuming part of control algorithm and reducing of computations intensity at the same performance is the main point for industry (it gives

possibility to use simple and inexpensive microprocessors),

- Reduction of common mode voltage,
- Good dynamics ,
- Reduction of acoustic noise (random modulation).

Basic performance indices which characterize *PWM* methods are summarized in Tab.3.1.

Table.3.1. Basic parameters of *PWM*.

lp.	Name of parameter	Symbol	Definition	Remarques
1	Modulation index	M	$M = U_{1m}/U_{1(six\text{-}step)} = U_{1m}/(2/\pi)U_d$	Two definition of modulation index are used. For sinusoidal modulation 0≤M≤0,785 or 0≤m≤1
		m	$m = U_m / U_{m(t)}$	
2	Max. linear range	M_{max}	0 ... 0.907	Depends on shape of modulation signal
		m_{max}	0 ... 1.154	
3	Overmodulation		$M > M_{max}$ $m > m_{max}$	Nonlinear range used for increase of output voltage
4	Frequency modulation ratio	m_f	$m_f = f_S / f_1$	For $m_f > 21$ asynchronous modulation is used
5	Switching frequency (number)	f_s (l_s)	$f_s = f_T = 1 / T_s$ T_s – sampling time	Constant
6	Total Harmonic Distortion	THD	THD=100%$* I_h / I_{s1}$	Used for voltage and current
7	Current distortion factor	d	$I_{h(rms)} / I_{h(six\text{-}step)(rms)}$	Independent of load parameters
8	Polarity consistency rule	PCR		Avoids ± 1 DC voltage transition

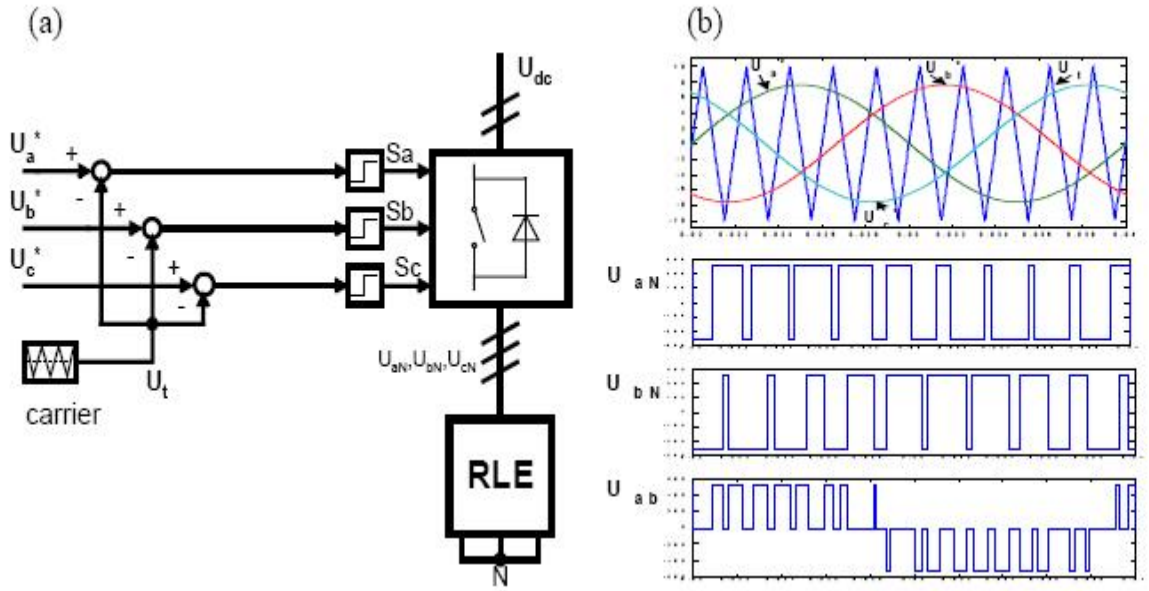

Fig. 3.5 (a) Scheme of carrier based sinusoidal modulation (*CB-SPWM*) (b) Basic waveforms

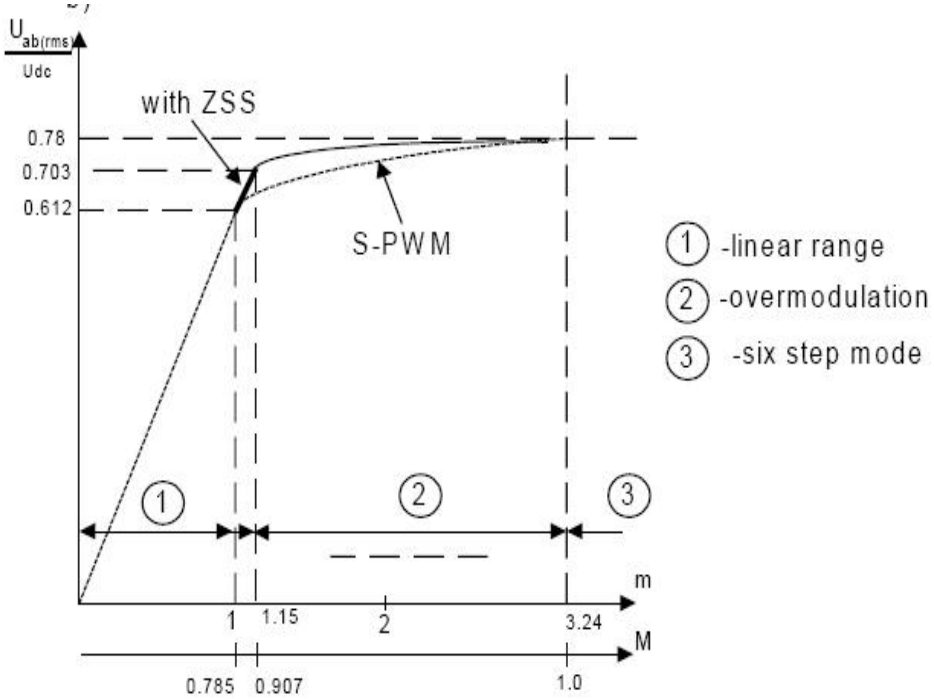

Fig. 3.6. Control characteristic of PWM converter

3.3.1. Carrier Based PWM

Sinusoidal modulation is based on triangular carrier signal. By comparison of common carrier signal with three reference sinusoidal signals Ua*, Ub*, Uc* (moved in phase of $2\pi/3$) the logical signals, which define switching instants of power transistor (Fig. 3.5) are generated. Operations with constant carrier signal concentrate voltage harmonics around switching frequency and multiple of switching frequency. Narrow range of linearity is a limitation for *CB-SPWM* modulator because modulation index reaches $Mmax = \pi/4 = 0.785$ ($m = 1$) only, e.g. amplitude of reference signal and carrier are equal. Over modulation region occurs above *Mmax* and *PWM* converter, which is treated like a power amplifier, operates at nonlinear part of characteristic (see Fig. 3.6).

Carrier Based - PWM with Zero Sequence Signal (ZSS)

If neutral point on AC side of power converter *N* is not connected with *DC* side midpoint *0* (Fig. 3.4), phase currents depend only on the voltage difference between phases. Therefore, it is possible to insert an additional Zero Sequence Signal (*ZSS*) of 3-th harmonic frequency, which does not produce phase voltage distortion *UaN*, *UbN*, *UcN* and without affecting load average currents (Fig. 3.8). However, the current ripple and other modulator parameters (e.g. extending of linear region to $Mmax = \pi / 2\ 3 = 0.907$, reduction of the average switching frequency, current harmonics) are changed by the *ZSS*. Added *ZSS* occurs between *N* and *0* points and is visible like a *UN0* voltage and can be observed in *Ua0*, *Ub0*, *Uc0* voltages (Fig. 3.8).

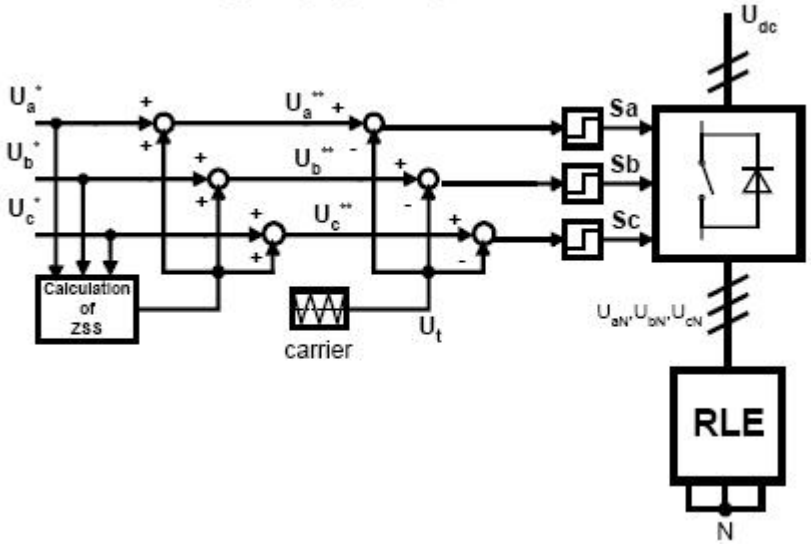

Fig. 3.7. Block scheme of modulator based on additional Zero Sequence Signal

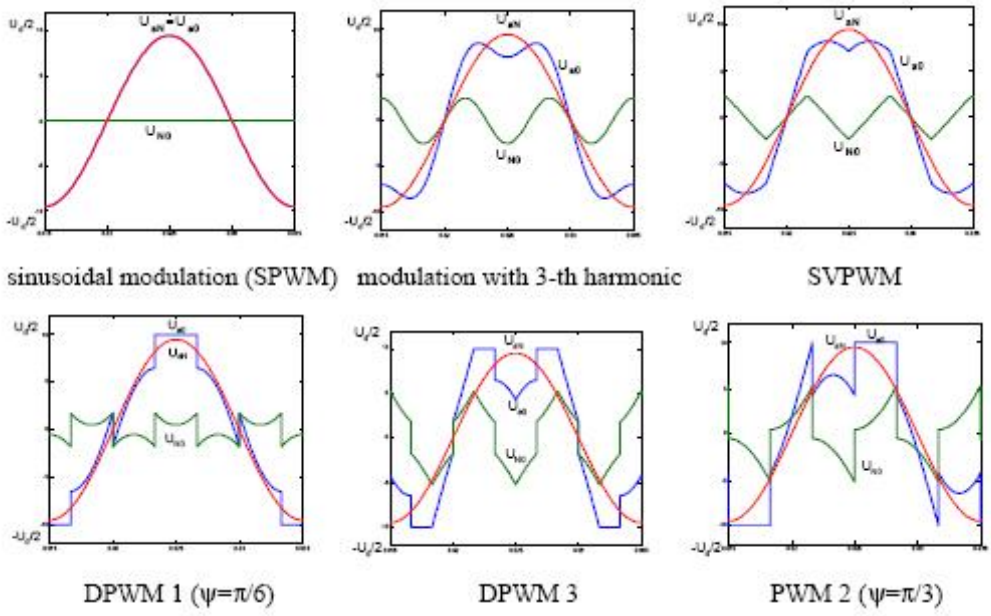

Fig. 3.8. Variants of PWM modulation methods in dependence on shape of ZSS.

Fig.3.8. presents different waveforms of additional *ZSS*, corresponding to different *PWM* methods. It can be divided in two groups: *continuous* and *discontinuous* modulation. The most known of continuous modulation is method with sinusoidal *ZSS* with 1/4 amplitude, it corresponds to minimum of output current harmonics, and with 1/6 amplitude it corresponds to maximal linear range. Triangular shape of *ZSS* with 1/4 peak corresponds to conventional (analogue) space vector modulation with symmetrical placement of zero vectors in sampling time (see Section 3.3.3). Discontinuous modulation is formed by unmodulated 60o segments (converter power switches do not switch) shifted from 0 to π/3 (different shift Ψ gives different type of modulation Fig. 3.9). It finally gives lower (average 33%) switching losses.

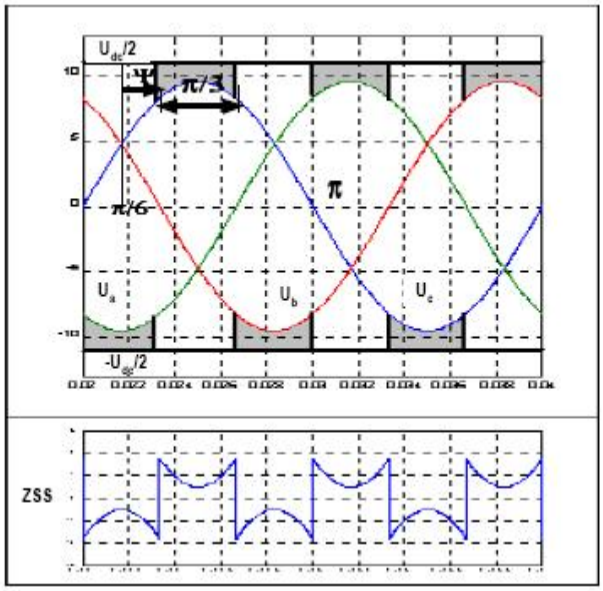

Fig. 3.9. Generation of ZSS for Discontinuous PWM method.

3.3.2. Space Vector Modulation (SVM)

The SVM strategy based on space vector representation (Fig. 3.10a) becomes very popular due to its simplicity. A three-phase two-level converter provides eight possible switching states, made up of six active and two zero switching states. Active vectors divide plane for six sectors, where a reference vector *U** is obtained by switching on (for proper time) two adjacent vectors. It can be seen that vector *U** (Fig. 3.10a) is possible to implement by the different switch on/off sequence of *U1* and *U2*, and that zero vectors decrease modulation index. Allowable length of *U** vector, for each of α angle, is equal *U*max =*Udc* / 3.

Contrary to *CB-PWM*, in the *SVM* there is no separate modulator for each phase. Reference vector *U** is sampled with fixed clock frequency *2fs = 1/Ts*, and next *U*(Ts)* is used to solve equations which describe times *t1, t2, t0* and *t7* (Fig. 4.12b). Microprocessor implementation is described with the help of simple trigonometrical relationship for first sector (3.17a and 3.17b), and, recalculated for the next sectors (n).

$$t_1 = \frac{2\sqrt{3}}{\pi} MT_S \sin(\pi/3-\alpha) \quad (3.17a)$$

$$t_2 = \frac{2\sqrt{3}}{\pi} MT_S \sin(\alpha) \quad (3.17b)$$

After *t1* and *t2* calculation, the residual sampling time is reserved for zero vectors *U0, U7* with condition $t1 + t2 \leq Ts$. The equations (3.17a), (3.17b) are identical for all variants of *SVM*. The only difference is in different placement of zero vectors *U0 (000)* and *U7 (111)*. It gives different equations defining *t0* and *t7* for each of method, but total duration time of zero vectors must fulfill conditions:

$$t_{0,7} = T_S - t_1 - t_2 = t_0 + t_7 \quad (3.18)$$

The neutral voltage between *N* and *0* points is equal: (see Tab. 3.2)

$$U_{N0} = (-\frac{U_{dc}}{2} t_0 - \frac{U_{dc}}{6} t_1 + \frac{U_{dc}}{6} t_2 + \frac{U_{dc}}{2} t_7) = \frac{U_{dc}}{2} \ (-t_0 - \frac{t_1}{3} + \frac{t_2}{3} + t_7) \quad (3.19)$$

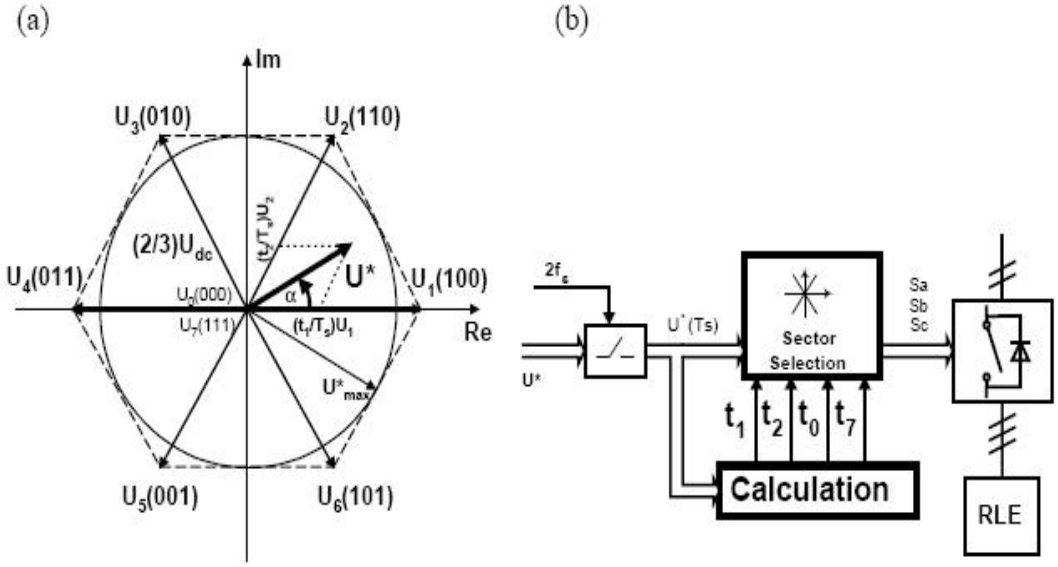

Fig. 3.10. (a) Space vector representation of three-phase converter,
(b) Block diagram of SVM

Table: 3.2. Voltages between *a, b, c* and *N, 0* for eight converter switching state

	U_{a0}	U_{b0}	U_{c0}	U_{aN}	U_{bN}	U_{cN}	U_{N0}
U_0	$-U_{dc}/2$	$-U_{dc}/2$	$-U_{dc}/2$	0	0	0	$-U_{dc}/2$
U_1	$U_{dc}/2$	$-U_{dc}/2$	$-U_{dc}/2$	$2U_{dc}/3$	$-U_{dc}/3$	$-U_{dc}/3$	$-U_{dc}/6$
U_2	$U_{dc}/2$	$U_{dc}/2$	$-U_{dc}/2$	$U_{dc}/3$	$U_{dc}/3$	$-2U_{dc}/3$	$U_{dc}/6$
U_3	$-U_{dc}/2$	$U_{dc}/2$	$-U_{dc}/2$	$-U_{dc}/3$	$2U_{dc}/3$	$-U_{dc}/3$	$-U_{dc}/6$
U_4	$-U_{dc}/2$	$U_{dc}/2$	$U_{dc}/2$	$-2U_{dc}/3$	$U_{dc}/3$	$U_{dc}/3$	$U_{dc}/6$
U_5	$-U_{dc}/2$	$-U_{dc}/2$	$U_{dc}/2$	$-U_{dc}/3$	$-U_{dc}/3$	$2U_{dc}/3$	$-U_{dc}/6$
U_6	$U_{dc}/2$	$-U_{dc}/2$	$U_{dc}/2$	$U_{dc}/3$	$-2U_{dc}/3$	$U_{dc}/3$	$U_{dc}/6$
U_7	$U_{dc}/2$	$U_{dc}/2$	$U_{dc}/2$	0	0	0	$U_{dc}/2$

Three-phase SVM with symmetrical placement of zero vectors (SVPWM)

The most popular *SVM* method is modulation with symmetrical zero states *SVPWM*):

$$t_0 = t_7 = \frac{(T_S - t_1 - t_2)}{2} \quad (3.20)$$

Figure 3.11a shows gate pulses for (*SVPWM*) and correlation between duty time *Ton*, *Toff* and duration of vectors *t1*, *t2*, *t0*, *t7*. For the first sector commutation delay can be computed as:

$$T_{aon} = \frac{t_0}{2} \qquad T_{aoff} = \frac{t_0}{2} + t_1 + t_2$$

$$T_{bon} = \frac{t_0}{2} + t1 \qquad T_{boff} = \frac{t_0}{2} + t_2 \quad (3.21)$$

$$T_{con} = \frac{t_0}{2} + t1 + t2 \qquad T_{coff} = \frac{t_0}{2}$$

For conventional *SVPWM* times *t1*, *t2*, *t0* are computed for one sector only. Commutation delay for other sectors can be calculated with the help of matrix:

$$\begin{bmatrix} Taoff \\ Tboff \\ Tcoff \end{bmatrix} = \text{Trans}$$

$$\begin{bmatrix} sector1 & sector2 & sector3 & Sector4 & sector5 & sector6 \\ 111 & 111 & 111 & 111 & 111 & 111 \\ 100 & 110 & 010 & 011 & 001 & 101 \\ 110 & 010 & 001 & 001 & 101 & 100 \end{bmatrix} \begin{bmatrix} 0.5To \\ t1 \\ t2 \end{bmatrix} \quad (3.22)$$

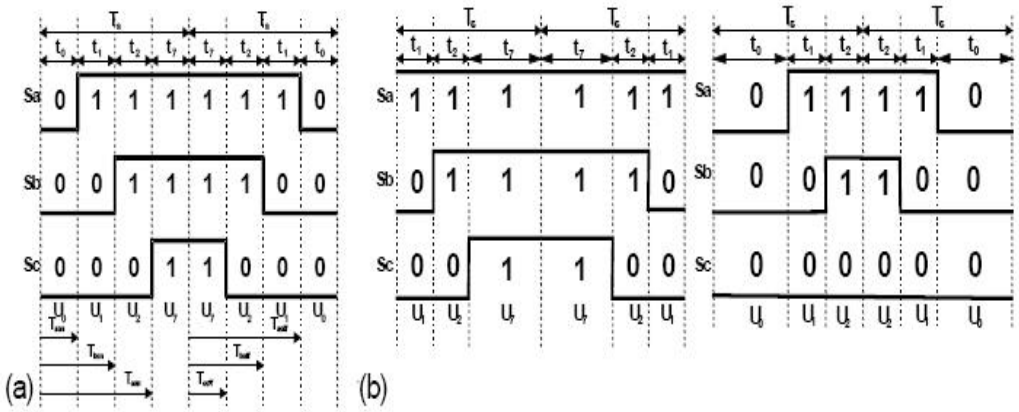

Fig. 3.11. Vectors placement in sampling time
a) three-phase SVM (*SVPWM, t0 = t7*) b) two-phase *SVM* (*DPWM, t0 = 0* and *t7 = 0*)

3.3.3 Carrier Based PWM versus Space Vector PWM

Comparison of *CB-PWM* methods with additional *ZSS* to *SVM* is shown on Fig. 3.13.Upper part shows pulse generation through comparison of reference signal *Ua **, Ub**, Uc*** with triangular carrier signal. Lower part of figure shows gate pulses generation in SVM (obtained by calculation of duration time of active vectors *U1, U2* and zero vectors *U0, U7*). It is visible that both methods generate identical gate pulses. Also it can be observed that the degree of freedom represented in selection of *ZSS* waveform in *CB-PWM*, corresponds to different placement of zero vectors *U0 (000)* and *U7 (111)* in sampling time *Ts = 1/2fs* of the *SVM*. Therefore, there is no exist difference between *CB-PWM* and *SVM*. The difference is only in the treatment of the three-phase quantities: CB-PWM operates in terms of three natural components, whereas *SVM* uses artificial (mathematically transformed) vector representation.

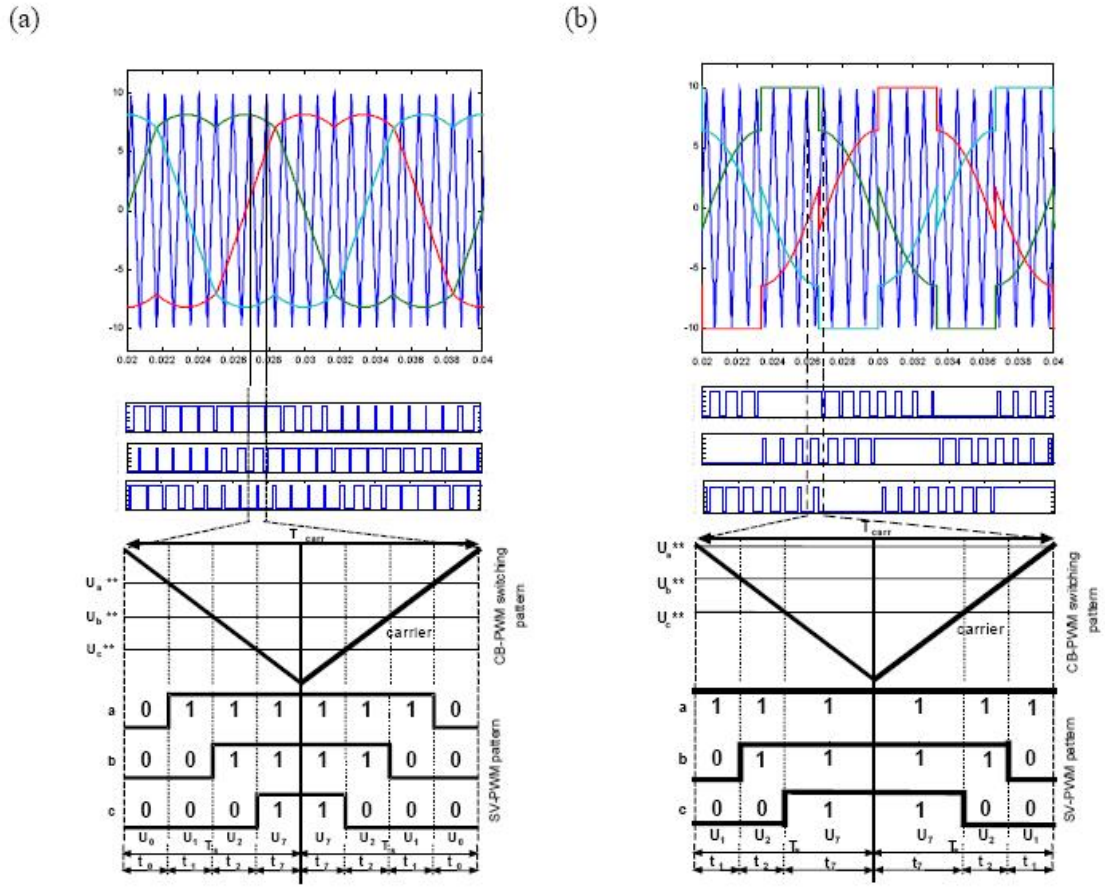

Fig. 3.12. Comparison of *CB-PWM* with *SVM* a) *SVPWM* b) *DPWM:*
From the top: *CB-PWM* with pulses, short segment of reference signal at high carrier frequency (reference signals are straight lines), formation of pulses in *SVM*.

Simulation based results are presented in Part-III

References

[1] Jagan Mohana Rao Malla and Manti Mariya Das, "Replace 48-Pulse GTO Converter by 9-Level GTO Converter in VSC DSTATCOM", International Journal of New Technologies in Science and Engineering (IJNTSE), Vol. 1, Issue. 1, pp. 1-14, Jan. 2014, www.ijntse.com

[2] Siva Ganesh Malla and Jagan Mohana Rao Malla, "Novel Controllers for 48-Pulse VSC SSSC Using Three Phase 9 Level Converter with One Transformer", International Journal of New Technologies in Science and Engineering (IJNTSE), Vol. 1, Issue. 2, pp. 1-18, May. 2014, www.ijntse.com

[3] Siva Ganesh Malla and Jagan Mohana Rao Malla, "Sensorless Control of Permanent Magnet Synchronous Motor (PMSM)", International Journal of New Technologies in Science and Engineering (IJNTSE), Vol. 1, Issue. 2, pp. 19-37, May. 2014, www.ijntse.com

[4] D. Jaya Deepu and Jagan Mohana Rao Malla, "Five level lowcost multilevel inverter fed DTC – SVM of induction motor", International Journal of New Technologies in Science and Engineering (IJNTSE), Vol. 1, Issue. 1, pp. 15-31, Jan. 2014, www.ijntse.com

[5] B. Srinu Naik, "Comparison of Direct and Indirect Vector Control of Induction Motor", International Journal of New Technologies in Science and Engineering (IJNTSE), Vol. 1, Issue. 1, pp. 110-131, Jan. 2014, www.ijntse.com

[6] Siva Ganesh Malla, "Secondary Battery as Source to Mobile Phone Battery", International Journal of New Technologies in Science and Engineering (IJNTSE), Vol. 1, Issue. 1, pp. 132-148, Jan. 2014, www.ijntse.com

[7] Jagan Mohana Rao Malla and Manti Mariya Das, "A Review on Direct Torque Control of Induction Motor", International Journal of New Technologies in Science and Engineering (IJNTSE), Vol. 1, Issue. 1, pp. 32-51, Jan. 2014, www.ijntse.com

[8] B.R. Krishna Tej, N.Sasank Sai and S.Deepak kumar, "Enhancing Productivity of a Roller Stand through Design Optimization using Manufacturing Simulation", International Journal of New Technologies in Science and Engineering (IJNTSE), Vol. 1, Issue. 1, pp. 52-60, Jan. 2014, www.ijntse.com

[9] Banothu Thavu, "Micro Controller based Current Fed Dual Bridge DC-DC Converter", International Journal of New Technologies in Science and Engineering (IJNTSE), Vol. 1, Issue. 1, pp. 61-81, Jan. 2014, www.ijntse.com

[10] T. Suneel, "Multi Level Inverters: A Review Report", International Journal of New Technologies in Science and Engineering (IJNTSE), Vol. 1, Issue. 1, pp. 82-109, Jan. 2014, www.ijntse.com